

Journal of Materials Chemistry A

Accepted Manuscript



This is an *Accepted Manuscript*, which has been through the Royal Society of Chemistry peer review process and has been accepted for publication.

Accepted Manuscripts are published online shortly after acceptance, before technical editing, formatting and proof reading. Using this free service, authors can make their results available to the community, in citable form, before we publish the edited article. We will replace this *Accepted Manuscript* with the edited and formatted *Advance Article* as soon as it is available.

You can find more information about *Accepted Manuscripts* in the [Information for Authors](#).

Please note that technical editing may introduce minor changes to the text and/or graphics, which may alter content. The journal's standard [Terms & Conditions](#) and the [Ethical guidelines](#) still apply. In no event shall the Royal Society of Chemistry be held responsible for any errors or omissions in this *Accepted Manuscript* or any consequences arising from the use of any information it contains.

Synthesis, optical and electrochemical properties of small molecules DMM-TPA[DTS(FBTTh₃)₃] and TPA[DTS(FBTTh₃)₃] and their application as donors for bulk heterojunction solar cells

Nara Cho,^a Sanhhyun Paek,^a Jihye Jeon,^b Kihyung Song,^b G. D. Sharma,^{*c} and Jaejung Ko^{*a}

^aDepartment of Materials Chemistry, Korea University, Chungnam 330-700, Republic of Korea. Fax: +82-44-860-1331; Tel: +82-44-860-1337; E-mail: jko@korea.ac.kr

^bDepartment of Chemical Education, Korea National University of Education, Chungbuk, 363-791, Republic of Korea

^cR & D center for Engineering and Science, JEC group of colleges, Jaipur Engineering College campus, Kukas, Jaipur (Raj.), India; E-mail: gdsharma273@gmail.com

*Corresponding authors

Abstract

Two symmetrical planar star-shaped organic small molecules **DMM-TPA[DTS(FBTTh₃)₃]** (**1**) and **TPA[DTS(FBTTh₃)₃]** (**2**) with fused TPA and TPA core donors, respectively and three branched DTS(FBTTh₃) units were synthesized and characterized. These small molecules were used donor materials along with PC₇₁BM acceptor for solution processed bulk heterojunction solar cells. The power conversion efficiency (PCE) of the solar cells based on **1** and **2** is about 2.87 % and 2.51 %, respectively, when the active layers were processed from CB solvent. The higher PCE of the solar cell based on **1** may be attributed to its low bandgap and broad absorption profile as compared to **2**. The PCE of the solution processed BHJ solar cells was improved up to 5.16 % and 4.70% for **1** and **2**, respectively, when active layers were processed with 4 v % DIO as additive in the CB solvent. The enhancement in the PCE was mainly due to the increase in J_{sc} and FF. The increase in the J_{sc} and FF is attributed to the balance charge transport between the electron and hole transport and reduction in the bimolecular recombination, leading to an increase in the PCE.

1. Introduction

Organic solar cells based on the bulk heterojunction active layer interpenetrating network of organic donor and fullerene derivative acceptor have attracted a great interest for the conversion of solar energy into electrical energy due to their advantages such as low cost of manufacturing through roll to roll processing, low weight and high mechanical flexibility [1]. Within a decade, the power conversion efficiency of these devices has been improved by three fold [2] and is still improving [3] due to a synergetic effort on the development of new donor and acceptor materials [4]. In last few years, there is a dramatic improvement in the organic BHJ solar cell performance with PCE surpassing 10 % using low band gap polymers as donor and fullerene as acceptor [5].

Small molecules BHJ solar cells offer several advantages over the polymer solar cells because of the easier synthesis of small molecules, less batch to batch variation and more reproducible performances of solar cells [6]. Hence considerable research effort has been focused on developing efficient small molecule materials for improved photovoltaic performance of device. Indeed, recently, the highest PCE above than 8 % have been reported by using solution processed small molecules [7], thus making them strong competitors for polymer solar cells.

Most of the small molecules as donor materials for photovoltaic applications normally contain four key constituents: donor /acceptor units, conjugated bridges, heteroatom substituents and side chains. The creative design and choice of donor or acceptor units, conjugated bridges and heteroatom substitutions has been successfully employed to overcome the shortcomings of unbalanced charge transport and poor film quality of small molecule based organic solar cells and shown high PCE [8]. Among the soluble small molecules, star shaped molecules have been developed as an interesting class of semiconducting materials and used in organic solar cells because of a number of advantages [9]. By tailoring and substituting the functional groups including donor units, acceptor units, and conjugated bridge, star shaped small molecules can be designed for low bandgap and strong and broader absorption, together with highly ordered and interconnected domain, resulting in higher PCEs of the organic solar cells [10]. Shang et al. have reported a symmetrical star shaped acceptor-donor-acceptor (A-D-A) small molecule comprising of a triphenylamine (TPA) core and various acceptors [11]. Inspired by their work, we have synthesized star type small molecules with TPA and DMM-TPA donor cores, for organic solar cells and achieved a PCE of 4.16 % [12]. We have also reported various symmetric and un-symmetric push-pull chromophores

for solution processed small molecule solar cells [13]. The use of push-pull type structure in small molecules enables efficient intramolecular charge transfer (ICT), providing better molar extinction coefficient and low bandgap. Moreover, an electron donating group such as TPA can play an important role in stabilizing the separated hole from an exciton and improving the hole transporting properties [14]. Recently, it was reported that fluorine substituted benzothiadiazole (BT) unit act as the effective electron withdrawing unit, producing a low bandgap semiconducting polymer and affording polymer solar cells with PCEs of 5-7 % [15]. The fluorine atom often affords the unique features that, when used in the BHJ active layer with fullerene derivative, boosts the intermolecular charge transfer through C-F---H interactions and thus affects photovoltaic performance of the solar cell. We have recently synthesized a novel fluorine substituted BT as core linked with electron donating TPA group through the π -conjugated bi-thiophene bridge based small molecules i.e. (bis[TPA-diTh]-MonoF-BT and (bis[TPA-diTh]-DiF-BT and used them as electron donor along with the PCBM as acceptor and yielded a PCE of 2.95 % [16].

Herein, we report the synthesis, characterization and photovoltaic characteristics of two novel symmetrical planar star shaped A-D-A organic semiconductors, i.e. **DMM-TPA[DTS(FBTTh₃)₃] (1)** and **TPA[DTS(FBTTh₃)₃] (2)**. Our strategy for choosing a fused amine as a core unit is to increase the lifetime of charge-separated state by the delocalization of the generated cation over a planar amine, leading to a high V_{oc} . For comparison, we synthesized a triphenyl amine derivative. The second novelty of this work is to compare the electron-acceptor moiety and its photovoltaic performance. These two small molecules were employed as donor materials for solution processed BHJ solar cells using PC₇₁BM as acceptor, yielding PCE of 2.87 % and 2.51 %, for **1** and **2**, respectively. Moreover, processing additive 1,8-diiodoctane (DIO), significantly affected the PCE of **1** or **2**:PC₇₁BM BHJ solar cells, achieving PCE of 5.16 % and 4.70% for **1** and **2**, respectively. The enhancement in PCE is mainly due to the higher values of J_{sc} and FF attributed to the increased crystallinity of the film and more balanced charge transport in the device. Therefore, we thought that if the electron acceptor is changed the PCE is enhanced. Indeed, the change of electron acceptor to F-substituted unit gave much improved PCE (5.19%). We have adapted long chain donor group to get a panchromatic visible spectrum. This one is another unique feature.

2. Experimental details

Measurements and Instruments

^1H NMR, ^{13}C NMR and ^{19}F NMR spectra were recorded on a Varian Mercury 300 spectrometer. Elemental analyses were performed with a Carlo Erba Instruments CHNS-O EA 1108 analyzer. Mass spectra were recorded on a JEOL JMS-SX102A instrument. The absorption and photoluminescence spectra were recorded on a Perkin-Elmer Lambda 2S UV-visible spectrometer and a Perkin LS fluorescence spectrometer, respectively. Cyclic voltammetry was carried out with a BAS 100B (Bioanalytical System, Inc.). A three electrode system was used and consisted of non-aqueous Reference Electrode (0.1 M Ag/Ag^+ acetonitrile solution; MF-2062, Bioanalytical System, Inc.), platinum working electrode (MF-2013, Bioanalytical System, Inc.), and a platinum wire (diam. 1.0 mm, 99.9 % trace metals basis, Sigma-Aldrich) as counter electrode. Redox potential of dyes was measured in CH_2Cl_2 with 0.1 M $(n\text{-C}_4\text{H}_9)_4\text{N-PF}_6$ with a scan rate between 50mVs^{-1} (vs. Fc/Fc^+).

Synthesis and Characterization of Materials:

The synthetic methods used are shown in Scheme 1. All reactions were carried out under an argon atmosphere. Solvents were distilled from appropriate reagents. All reagents were purchased from Sigma-Aldrich, TCI and Alfa Aesar. 5-Fluoro-4,7-diiodobenzo[*c*][1,2,5]thiadiazole (**A**), trimethyl-[5"-*n*-hexyl (2,2';5',2"-terthiophene)-5-yl]stannane (**B**)², 2,6,10-trimethylstannyl-4,4,8,8,12,12-hexamethyl-4*H*,8*H*,12*H*-benzo[1,9]quinolizino[3,4,5,6,7,-*defg*] acridine (**F**)², tris(4-(trimethylstannyl) phenyl)amine (**G**) were synthesized using a modified procedure of previous references [16, 17].

4-Iodo-5-fluoro-7-[5"-*n*-hexyl-(2,2';5',2"-terthiophene)-5-yl]-benzo[*c*][1,2,5]thiadiazole (**C**)

In a 125 mL flame-dried 2-neck round-bottom flask with a condenser, 5-fluoro-4,7-diiodobenzo[*c*][1,2,5]thiadiazole¹ (**A**, 2.44 g, 6.01 mmol), trimethyl-[5"-*n*-hexyl (2,2';5',2"-terthiophene)-5-yl]stannane² (**B**, 3.7 g, 6.01 mmol) and anhydrous toluene 80 mL were added. The mixture was then purged with nitrogen gas. Then, $\text{Pd}(\text{PPh}_3)_4$ (0.2 g, 0.17 mmol) was added and the reaction mixture was heated to reflux for 2 days. The reaction mixture was then cooled to room temperature and the solvent was evaporated. The red-brown product was purified by column chromatography (silica gel, chloroform: petroleum ether=1:2) as eluent. Yield: 50 % Mass: m/z 609.59 [M^+]. ^1H NMR (300 MHz, CDCl_3): δ 8.00 (d, 1H, $^3J = 3.9$ Hz), 7.58 (d, 1H, $^3J = 9.6$ Hz), 7.17 (d, 1H, $^3J = 3.9$ Hz), 7.14 (d, 1H, $^3J = 3.6$ Hz), 7.00 (dd, 2H, $^3J = 3.9, 3.3$ Hz), 6.69 (d, 1H, $^3J = 3.9$ Hz), 2.82 (t, 2H, $^3J = 7.2$ Hz), 1.71 (t, 2H, $^3J = 6.3$ Hz), 1.39 (m, 6H), 0.92 (t, 3H, $^3J = 6.9$ Hz). ^{13}C NMR (75 MHz, CDCl_3): δ 165.85, 162.54, 156.67, 156.53, 147.64, 146.10, 140.49, 137.99, 135.45, 134.61, 134.21, 129.99,

128.06, 127.91, 125.17, 124.99, 124.26, 123.73, 115.03, 114.60, 31.75, 30.39, 29.88, 28.96, 22.78, 14.31. ^{19}F NMR (280 MHz, CDCl_3): δ -89.98 ppm

4-[3,3'-Dihexylsilylene-2,2'-bithiophene]-5-fluoro-7-[5''-n-hexyl-(2,2';5',2''-terthiophene)-5-yl]-benzo[c][1,2,5]thiadiazole (D)

In a 125 mL flame-dried 2-neck round-bottom flask with a condenser, 4-iodo-5-fluoro-7-[5''-n-hexyl-(2,2';5',2''-terthiophene)-5-yl]-benzo[c][1,2,5]thiadiazole¹ (C, 2.59 g, 4.24 mmol), tributyl-[3,3'-dihexylsilylene-2,2'-bithiophene-5-yl]stannane² (2.88 g, 6.24 mmol) and anhydrous toluene 80 mL were added. The mixture was then purged with nitrogen gas. Then, $\text{Pd}(\text{PPh}_3)_4$ (0.12 g, 0.1 mmol) was added and the reaction mixture was heated to reflux for 1 day. The reaction mixture was then cooled to room temperature and the solvent was evaporated. The purple product was purified by column chromatography (silica gel, dichloromethane:hexane=1:4) as eluent. Yield: 75 % Mass: m/z 844.35 [M^+]. ^1H NMR (300 MHz, CDCl_3): δ 8.27 (s, 1H), 8.03 (d, 1H, $^3J = 3.9$ Hz), 7.76 (d, 1H, $^3J = 12.9$ Hz), 7.29 (d, 1H, $^3J = 4.5$ Hz), 7.23 (d, 1H, $^3J = 3.6$ Hz), 7.18 (d, 1H, $^3J = 3.9$ Hz), 7.11 (d, 1H, $^3J = 4.5$ Hz), 7.04 (d, 1H, $^3J = 3.9$ Hz), 7.01 (d, 1H, $^3J = 3.6$ Hz), 6.70 (d, 1H, $^3J = 3.9$ Hz), 2.82 (t, 2H, $^3J = 6.9$ Hz), 1.71 (t, 2H, $^3J = 6.9$ Hz), 1.44 (m, 24H), 1.00 (m, 11H). ^{13}C NMR (75 MHz, CDCl_3): δ 160.27, 156.93, 153.48, 149.82, 149.27, 146.12, 143.01, 142.27, 139.76, 137.82, 136.69, 135.10, 134.44, 133.36, 129.93, 129.10, 126.34, 125.06, 125.03, 124.41, 123.85, 123.76, 116.19, 33.03, 31.72, 31.61, 30.36, 28.91, 24.33, 22.73, 14.25, 12.08. ^{19}F NMR (280 MHz, CDCl_3): δ -108.11 ppm

4-[5-Bromo-3,3'-dihexylsilylene-2,2'-bithiophene]-5-fluoro-7-[5''-n-hexyl-(2,2';5',2''-terthiophene)-5-yl]-benzo[c][1,2,5]thiadiazole (E)

4-[3,3'-Dihexylsilylene-2,2'-bithiophene]-5-fluoro-7-[5''-n-hexyl-(2,2';5',2''-terthiophene)-5-yl]-benzo[c][1,2,5]thiadiazole (D, 0.45 g, 0.53 mmol) was dissolved in 50 mL of CHCl_3 . Then, *n*-bromosuccinimide (0.11 g, 0.64 mmol) was added by portions and the mixture was stirred for 24 h at room temperature under dark condition. The organic layer was separated and dried over anhydrous magnesium sulfate. The solvent was removed in vacuo. The product was purified by column chromatography. Yield: 65 % Mass: m/z 923.24 [M^+]. ^1H NMR (300 MHz, CDCl_3): δ 8.20 (s, 1H), 7.92 (d, 1H, $^3J = 3.9$ Hz), 7.62 (d, 1H, $^3J = 13.8$ Hz), 7.21 (d, 1H, $^3J = 3.6$ Hz), 7.16 (d, 1H, $^3J = 3.6$ Hz), 7.12 (dd, 1H, $^3J = 2.7, 3.3$ Hz), 7.04 (s, 1H), 6.96 (d, 1H, $^3J = 3$ Hz), 6.66 (s, 1H), 2.80 (m, 2H), 1.67 (m, 2H), 1.44 (m, 24H), 1.00 (m, 11H). ^{13}C NMR (75 MHz, CDCl_3): δ 160.68, 157.46, 153.30, 149.72, 145.21,

145.15, 142.98, 142.22, 139.71, 136.92, 135.72, 134.99, 134.41, 133.84, 133.29, 131.72, 129.91, 129.46, 129.27, 128.12, 127.63, 126.34, 124.62, 123.99, 116.29, 107.04, 33.27, 33.05, 32.68, 31.83, 31.45, 31.19, 30.36, 30.22, 28.94, 24.36, 23.13, 22.74, 17.91, 12.08. ^{19}F NMR (280 MHz, CDCl_3): δ -107.84 ppm

Tris[[4-[3,3'-dihexylsilylene-2,2'-bithiophene]-5-fluoro-7-[5''-n-hexyl-(2,2';5',2''-terthiophene)-5-yl]-benzo[c][1,2,5]thiadiazole]-2,6,10-yl]-4,4,8,8,12,12-Hexamethyl-4H,8H,12Hbenzo[1,9]quinolizino[3,4,5,6,7,-defg]acridine (DMM-TPA[DTS(FBTTh₃)₃], 1)

4-[5-Bromo-3,3'-dihexylsilylene-2,2'-bithiophene]-5-fluoro-7-[5''-n-hexyl-(2,2';5',2''-terthiophene)-5-yl]-benzo[c] [1,2,5] thiadiazole (**E**, 0.35 g, 0.38 mmol), 2,6,10-trimethylstannyl-4,4,8,8,12,12-hexamethyl-4H,8H,12H-benzo[1,9] quinolizino [3,4,5,6,7,-defg]acridine (**F**, 0.092 g, 0.11 mmol), $\text{Pd}(\text{PPh}_3)_4$ (0.06 g, 0.052 mmol), and anhydrous toluene (40 ml) were added to a 125 mL flame-dried 2-neck round-bottom flask with a condenser under a nitrogen atmosphere. The reaction mixture was heated to reflux for 2 days. The reaction mixture was then cooled to room temperature. The organic layer was separated and dried over anhydrous magnesium sulfate. The solvent was removed in vacuo. The purple product was purified by column chromatography. Yield: 40 % Mass: m/z 2894.50 [M^+]. ^1H NMR (300 MHz, CDCl_3): δ 8.31 (s, 1H), 8.03 (d, 1H, $^3J = 3.6$ Hz), 7.77 (d, 1H, $^3J = 14.1$ Hz), 7.66 (dd, 2H, $^3J = 6.9$ Hz), 7.16 (m, 3H), 7.01 (dd, 1H, $^3J = 2.5, 3.3$ Hz), 6.69 (s, 1H), 2.79 (m, 2H), 1.78 (m, 2H), 1.45 (m, 24H), 1.04 (m, 11H). ^{13}C NMR (75 MHz, CDCl_3): δ 160.11, 156.76, 153.35, 149.73, 146.01, 145.12, 144.62, 141.52, 139.62, 137.69, 136.64, 135.06, 134.38, 133.53, 133.24, 130.54, 129.41, 128.97, 126.76, 124.99, 124.31, 123.75, 121.22, 116.50, 111.96, 106.97, 33.11, 31.64, 31.16, 30.31, 30.17, 29.83, 28.91, 24.93, 24.67, 24.38, 24.13, 23.83, 22.78, 14.28, 12.13, 1.13. ^{19}F NMR (280 MHz, CDCl_3): δ -108.04 ppm
Anal. Calc. for $\text{C}_{159}\text{H}_{168}\text{F}_3\text{N}_7\text{S}_{18}\text{Si}_3$: C, 65.95; H, 5.85; N, 3.39. Found : C, 65.93; H, 5.84; N, 3.38.

Tris[[4-[3,3'-Dihexylsilylene-2,2'-bithiophene]-5-fluoro-7-[5''-n-hexyl-(2,2';5',2''-terthiophene)-5-yl]-benzo[c][1,2,5]thiadiazole]-p-phenylene]amine (TPA[DTS(FBTTh₃)₃], 2)

4-[5-Bromo-3,3'-dihexylsilylene-2,2'-bithiophene]-5-fluoro-7-[5''-n-hexyl-(2,2';5',2''-terthiophene)-5-yl]-benzo [c] [1,2,5]thiadiazole (**E**, 0.33 g, 0.36 mmol), tris(4-(trimethylstannyl)phenyl)amine (**G**, 0.075 g, 0.1 mmol), $\text{Pd}(\text{PPh}_3)_4$ (0.06 g, 0.052 mmol), and anhydrous toluene (40 ml) were added to a 125 mL flame-dried 2-neck round-bottom flask

with a condenser under a nitrogen atmosphere. The reaction mixture was heated to reflux for 2 days. The reaction mixture was then cooled to room temperature. The organic layer was separated and dried over anhydrous magnesium sulfate. The solvent was removed in vacuo. The purple product was purified by column chromatography. Yield: 40 % Mass: m/z 2774.31 $[M^+]$. 1H NMR (300 MHz, $CDCl_3$): δ 8.21 (s, 1H), 8.07 (d, 2H, $^3J = 3.9$ Hz), 7.72 (d, 1H, $^3J = 14.1$ Hz), 7.79 (d, 2H, $^3J = 6.8$ Hz), 7.19 (m, 3H), 7.08 (dd, 1H $^3J = 2.6, 3.5$ Hz), 6.66 (s, 1H), 2.78 (m, 2H), 1.79 (m, 2H), 1.44 (m, 24H), 1.04 (m, 11H). ^{13}C NMR (75 MHz, $CDCl_3$): δ 161.14, 157.74, 154.36, 150.71, 147.03, 146.14, 145.65, 142.55, 139.89, 138.67, 137.63, 136.04, 135.39, 134.51, 134.25, 131.61, 129.87, 128.99, 127.75, 125.04, 124.86, 124.65, 122.21, 117.51, 112.82, 107.78, 33.14, 31.66, 31.21, 30.30, 30.25, 29.85, 28.90, 24.91, 24.64, 24.37, 24.15, 23.81, 22.77, 14.25, 12.14, 1.15. ^{19}F NMR (280 MHz, $CDCl_3$): δ -107.93 ppm. Anal. Calc. for $C_{150}H_{156}F_3N_7S_{18}Si_3$: C, 64.92; H, 5.67; N, 3.53. Found : C, 64.90; H, 5.66; N, 3.52.

Device fabrication and characterization

The BHJ organic solar cells were prepared using the indium tin oxide (ITO) coated glass substrate as anode, Al as cathode and a blended film of donor :PC₇₁BM between the two electrodes as photoactive layer as follow: Firstly, ITO coated glass substrates were cleaned with detergent, ultrasonicated in acetone and isopropyl alcohol, and subsequently dried in an oven for 12 hr. An aqueous solution of PEDOT:PSS (Heraeus, Clevious P VP, Al 4083) in aqueous solution was spin cast on the ITO substrates obtaining a film of about 40 nm thick. The PEDOT:PSS film was then dried for 10 min at a temperature of 120° C in ambient conditions. Then, a 20 mg/mL solution of donor /PC₇₁BM blends in different solvents were prepared with different weight ratio and then spun cast on the top of PEDOT:PSS layer and then dried at 80° C for 10 min. The solvents include chlorobenzene (CB) and CB containing (1, 2, 3, 4 and 5 % v) 1,8-diiodooctane (DIO). The thickness of the photoactive is about 100 ±10 nm. Finally ~ 90 nm thick Al electrode was deposited on the top of BHJ film under reduced pressure (<10⁻⁶ Torr). . All the devices were fabricated and tested in ambient atmosphere without encapsulation. The active area of the devices is about 0.20 cm². The hole only and electron only devices ITO / PEDOT:PSS /donor:PC₇₁BM/Au and Al/donor:PC₇₁BM/Al structures, were fabricated to measure the hole and electron mobility, respectively.

The current–voltage characteristics of the devices were measured using a computer controlled Keithley 238 source meter in dark as well as under illumination intensity of 100

mW/cm². A xenon light source coupled with AM1.5 optical filter was used as light source to illuminate the surface of the devices. The incident photon to current efficiency (IPCE) of the devices was measured illuminating the device through the light source and monochromator and resulting current was measured using Keithley electrometer under short circuit condition.

3. Results and discussion

Optical and electrochemical properties

Figure 1a and 1b show the UV-visible absorption spectra of **1** and **2** in both CB solution and thin film form. The corresponding optical properties are summarized in Table 1. The absorption spectra of both small molecules exhibited two typical transition bands in the 300 -700 nm region. The absorption band in the lower wavelength regions with absorption peak at 413 nm and 406 nm for **1** and **2**, respectively, were assigned to the π - π^* transition. The absorption band in longer wavelength region with absorption maxima at wavelength 575 nm and 564 nm for **1** and **2**, respectively can be assigned to intramolecular charge transfer (ICT) transition between the donor and acceptor units. The π - π^* transition and ICT transition bands of **1** showed a slight redshift as compared to those of the titled star shaped **2**, indicating that the planar structure of **1** results in more efficient ICT and π - π^* transitions and facilitates intermolecular π - π packing interactions more efficiently than the titled shaped structure **2**. The absorption band in the wavelength range 450 -750 nm is attributed to the ICT transition bands between HOMO and LUMO. These bands were further analyzed by time dependent density functional theory (TD-DFT) calculations using the B3LYP functional/6-31G* basis set. Figure S1 and Table S1 show the calculated energy bands of these materials in vacuo (see the supporting information). In thin film, the absorption bands of **1** and **2** showed a redshift relative to those in solution, and broader spectral bands, may be caused by the existence of π - π stacking of molecules in dense states. As the absorption edges of the **1** and **2** are 768 nm and 724 nm, respectively. The optical bandgap (E_g^{opt}) are calculated as 1.61 eV and 1.73 eV, for **1** and **2**, respectively. Both the small molecules exhibit a broader absorption range and low bandgap, which would be in favor of light harvesting when used as photoactive layer materials in organic solar cells.

The HOMO and LUMO energy levels of the both small molecules were estimated from the oxidation and reduction onsets, respectively, observed in cyclic voltammograms (CV) under the assumption that the energy levels of ferrocene (Fc) was 4.8 eV below the vacuum level and shown in Table 1. The HOMO/ LUMO energy levels of **1** and **2** were

calculated as -4.8381/-3.744 eV and -4.8869/-3.471 eV, respectively. The values of the HOMO energy levels of these small molecules are slightly decreased as compared to the small molecules without fluorine substituted BT [12], indicating that the substitution of electron withdrawing fluorine in BT decreases the HOMO energy level. Considering that the PC₇₁BM has HOMO and LUMO levels around 6.2 eV and 4.0 eV, respectively, **1** and **2** can be used as donor materials and PC₇₁BM as acceptor material and their energy levels will be compatible with PC₇₁BM, for efficient exciton dissociation in BHJ organic solar cells.

Theoretical calculations and molecule simulation

The electronic properties of the **1** and **2** have also investigated by theoretical calculations. Figure S1 (supplementary information) shows the optimized structures of **1** and **2**, which were calculated by TD-DFT using the B3LYP functional/6-31G* basis set. The orbital densities of the HOMOs of **1** and **2** were evenly distributed on triarylamine core. But the orbital densities of LUMOs and LUMO+1 of these materials were located on benzothiadiazole moiety. The calculations revealed that the intramolecular charge transfer (ICT) from triarylamine core (HOMO state) to benzothiadiazole core (LUMO and LUMO+1 state) can effectively occur in **1** and **2** when excited by light energy. The details are summarized in Table S1 in the Supporting Information.

Hole mobility in pristine **1** and **2**

Hole mobility is another important parameters of the small molecules for the photovoltaic applications. In this study, we investigated the hole mobility of **1** and **2** by space charge limited current (SCLC) model with a device structure of ITO/PEDOT:PSS/ **1** or **2**/Au [17]. For hole only device, SCLC is described by [18]

$$J_{SCLC} = \frac{9}{8} \varepsilon_r \varepsilon_o \mu_o \frac{(V - V_{bi})^2}{d^3} \exp\left[0.89\gamma \sqrt{\frac{V - V_{bi}}{d}}\right] \text{----- (1)}$$

where J_{SCLC} stands for current density, d is the thickness of the active layer, $V = V_{appl} - V_{bi}$, V_{bi} is the built in potential. The results are plotted as $\ln(J_d/V^2)$ versus (V/d) and the hole mobilities are evaluated to be $4.56 \times 10^{-5} \text{ cm}^2/\text{Vs}$ and $7.56 \times 10^{-5} \text{ cm}^2/\text{Vs}$, for **2** and **1** respectively. The planar structure of **1** that results in enhanced hole transport via efficient intermolecular π - π packing interactions leads to its higher hole mobility.

Photovoltaic properties

We have explored the photovoltaic properties of the organic solar cells based on two small molecules as electron donor along with PC₇₁BM as acceptor by fabricating BHJ devices with the structure of ITO/PEDOT:PSS/ **1** or **2**: PC₇₁BM/ Al. PC₇₁BM instead of PC₆₁BM was chosen as the electron acceptor due to its stronger absorption in the visible region. We have fabricated the devices with different weight ratio ranging for 1:1 to 1:4 and found that the optimized ratio is 1:2. The photovoltaic parameters of the devices with different weight ratios are summarized in Table S2 (supporting information). Figure 2a and 2b shows the J-V characteristics of optimized devices under stimulated AM1.5 radiation (100 mW/cm²). The BHJ devices based on **1** and **2** small molecules processed from CB showed a PCE of 2.87 % (J_{sc}= 9.18 mA/cm², V_{oc}= 0.68 V and FF = 0.46) and 2.44 % (J_{sc} = 8.54 mA/cm², V_{oc} = 0.68 V and FF 0.42), respectively. The relatively higher value of J_{sc} and FF for device based on **1** could be attributed to the higher hole mobility resulting from efficient intermolecular π-π packing interactions, which is in turn more efficient for planar core DMM-TPA unit of **1**. The value of V_{oc} of the devices based on both small molecules is same, that is consistent their similar value of HOMO level, since the V_{oc} for BHJ solar cell is difference between the HOMO level of donor and LUMO level of PC₇₁BM.

The IPCE values of the devices were estimated from following expression:

$$IPCE(\%) = \frac{1240J_{sc}}{\lambda P_{in}} \text{-----} (2)$$

Where J_{sc} (mA/cm²) is the photocurrent under short circuit condition, λ (nm) is the wavelength of monochromatic incident light and P_{in} (mW/cm²) is the irradiance flux. The IPCE spectra of the devices based on **1** and **2** are shown in Figure 3a and 3b, respectively. The IPCE values are higher and spectrum is boarder for device based on **1** than that for **2**. The higher value of J_{sc} for device based on the **1** than **2** is consistent with the IPCE spectra.

Photoluminescence (PL) spectroscopy has been used to get information about the exciton dissociation efficiency and mixing morphology of the blend active layer used in the device. The PL spectra of pristine **1** and **2** and their blend with PC₇₁BM are shown in Figure 4a and 4b. It can be seen that in the blends the PL intensity is significantly quenched. The PL intensities of the small molecules are quenched 84 % and 78 % for **1**:PC₇₁BM and **2**:PC₇₁BM blends, respectively. Higher PL quenching for **1**:PC₇₁BM blend as compared to **2**:PC₇₁BM blend indicates that the probability for an exciton to reach the D/A interfaces and exciton

dissociation, decrease from **2** to **1** active blends. This behavior is correlated with the difference of IPCE and J_{sc} values of devices.

The PCE of the BHJ using **1** or **2** as donor and PC₇₁BM as acceptor is low and may be due to the low FF and J_{sc} . These two photovoltaic parameters depend upon the nanoscale morphology of the active layer and balance charge transport in the devices. Various processing techniques have been developed in order to optimize the nanoscale morphology of the BHJ active layer to improve the PCE of organic solar cells, including thermal annealing [19], solvent annealing [20] and spontaneous inter-diffusion of bi-layer heterojunction [21]. In addition to above processing methods, recently, the use of solvent additives was employed to enhance the photovoltaic performance of BHJ organic solar cells [22]. This technique is very useful to control the morphology of BHJ active layer where thermal annealing is undesirable or ineffective. It has been reported that morphology of active layer can be controlled by incorporating a few percentage of solvent additives to the blend solution and is the effective approach to improve the PCE of the organic solar cells based on several polymeric donors [23]. It was reported that the solvent additives also improves the photovoltaic performance of organic solar cells with solution processed small molecules [6a, 24]. Solvent additives (usually with poor solubility and high boiling point) allows the polymer chains to aggregate easily while main solvent is evaporated during the film formation using spin coating technique, and hence facilitate the crystallization process. It was reported that in small molecule BHJ systems, the main function of the DIO additive is to affect the nanoscale morphology [25]. The enhancement in the PCEs has been ascribed to the controlling of crystallization behaviour of the donor materials within the blend films, resulting in optimized domain sizes.

In organic BHJ solar cells, after the absorption of photons from incident light, excitons are generated either in donor or acceptor or in both, and then diffuse towards the donor/acceptor interface where ultra-fast photoinduced charge transfer occurs, and thereby generates free holes and electrons in donor and acceptor phases, respectively. These free charge carriers are swept out by internal built in field towards the electrodes. During this process the collection of the charge carriers by the electrodes must be fast, otherwise, recombination might take place within the active layer [26].

To improve the PCE organic devices based on **1** and **2**, we have used 1, 8-diiodooctane (DIO) as additive. We have varied the concentration of DIO in the solvent from 1 % to 5 % by volume and found that the optimized concentration was about 4 % v (the

photovoltaic parameters are summarized in Table S3 supplementary information). When the concentration increased beyond 4 % v, the PCE of the solar cell decreases may due to the over aggregation of donor phase, which disturbs the percolating pathways of acceptor phase and reduces the electron mobility in the BHJ active layer. The over-aggregation of the donor phase may also reduce the effective interfacial area for charge separation and consequently reduces the photocurrent generation [25]. The reduction in PCE may also be attributed to the incomplete drying of active layer due to the high boiling point of DIO. Therefore, we have discussed the effect of solvent additive on the photovoltaic performance of the devices, only for the 4 % DIO by volume in CB. The J-V characteristic of the devices processed with DIO/DCB, under illumination are shown in Figure 2a and 2b and the corresponding photovoltaic parameters are compiled in table 2. The PCE of the devices for **1** and **2** have been significantly enhanced up to 5.16 % and 4.70 %, respectively. The increase in the PCE upon addition of DIO arises from the enhancement in FF and J_{sc} .

The FF of the BHJ solar cells cast without additive is low may be due to the build up of the space charge due to the imbalance in the hole and electron transport in the device [27]. Though, at short circuit condition the charge transport may not limit extraction, a reduced hole or electron mobility may lead to a build up of space charge within the devices and increased bimolecular recombination at low internal fields, leading to the poor FF. To get information about this, we have measured the hole and electron mobilities in each blend using single carrier diodes using charge selective contacts [28]. Hole only devices were fabricated for different blends of the solar cells, with structure ITO/PEDOT:PSS/**1** or **2**:PC₇₁BM (processed with CB or DIO/CB solvent /Au. Au was selected, since its work function is significantly deep enough to prevent injection of electrons into the LUMO of PC₇₁BM [29]. The electron only devices were fabricated with the structure Al/**1** or **2**:PC₇₁BM/Al. The hole mobilities of **1** and **2** in the blend films with and without DIO additive extracted from the space charge limited current (SCLC) obtained in dark for hole only devices using Figure 5b and show the dark J-V characteristics of ITO/PEDOT:PSS/**1**:PC₇₁BM processed with and without DIO/Au. Similar results have been observed for devices based on **2**:PC₇₁BM blends. To estimate the hole and electron mobilities in the blend with and without DIO additive, the J-V characteristics of the respective devices were fitted to the SCLC as described in Eq (1). The hole mobilities extracted from the J-V characteristics for the blends cast without and with DIO are $4.78 \times 10^{-6} \text{ cm}^2/\text{Vs}$ for **1** and $3.21 \times 10^{-6} \text{ cm}^2/\text{Vs}$ for **2**, and $5.6 \times 10^{-5} \text{ cm}^2/\text{Vs}$ for **1** and $1.2 \times 10^{-5} \text{ cm}^2/\text{Vs}$ for **2**, respectively. The

increase in the hole mobility with the DIO additive agrees with the results revealed by the morphology change, in which the domain size and crystallinity increases with the addition of DIO in the solvent. The electron mobilities (estimated from the Fig. 5b) of the blend films processed with CB and DIO (4 v %) /CB are quite similar, 3.4×10^{-4} and 2.87×10^{-4} cm^2/Vs for both **1** and **2**, respectively. The electron and hole mobilities are more balanced in the BHJ active layer processed with DIO/CB solvent. The more balanced charge transports may be one of the possible reasons that contribute to the higher J_{sc} , and FF, and thereby resulting in enhanced IPCE and PCE of the DIO/DCB processed devices.

The FF of the BHJ organic solar cells depends upon the charge recombination occurred within the devices [30]. To get information about the effect of the DIO additive on the charge recombination and photoinduced carrier generation rate, we have plotted the photocurrent ($J_{\text{ph}} = J_{\text{light}} - J_{\text{dark}}$) against the effective internal voltage V_{in} , i.e., $(V_{\text{o}} - V_{\text{appl}})$, where V_{o} is the voltage when photocurrent is zero (as shown in Fig. 6). This effective voltage determines the strength of the electric field within the device and thus driving force for charge extraction [31]. As shown in figure 6, J_{ph} increases linearly at low V_{in} , and saturates at high voltage around 2.2 V and above. It can be seen from figure 6 that the photocurrent in the BHJ device processed from with DIO additive quickly saturates at a low effective voltage about 0.8 V. This indicates that the charge generation and extraction processes are relatively independent of the electric field. In contrast, the photocurrent in the devices cast from CB only does not even begin to saturate even up to 2.2 V. This indicates that in the device cast from the CB, the formation of space charge limits the charge extraction. For this device limited by the insufficient extraction, the high densities of charges lead to significantly increased bimolecular recombination and thus low FF.

The morphology of the photoactive blend film has a significant influence on the charge separation and transport in the device and investigated by atomic force microscopy (AFM) in tapping mode. The AFM images of the **1**: PC₇₁BM blend films processed from CB and DIO/CB solvent are shown in Fig. 7. Similar AFM images have been observed for **2**:PC₇₁BM blends. It can be seen from the AFM images (Fig. 7) that the blend film processed with CB shows that **1** and PC₇₁BM are homogeneously mixed and the surface is very smooth (with surface roughness of 0.42 nm) and does not show any significant phase separation and domain size about 2- 3 nm. These too small domain size leads to reduced performance because of increased recombination. The addition of 4 % of DIO in the solvent shows significant change in the morphology of the blend film (with surface roughness of 2.18 nm).

The observed domain size is about 15-25 nm. The larger roughness film is indicative of a more highly ordered structure which indicates more efficient charge separation in the OSC [32, 33]. Moreover, the electron and hole mobilities are more balanced in the film processed with 4 % DIO/ CB [33]. The effectiveness of DIO may be linked with its ability to selectively dissolve PC₇₁BM aggregates in solution [34]. Domain larger than ~ 20 nm are generally are not beneficial to device performance as the limited exciton diffusion length of most of the organic semiconductors is about 10 -15 nm, requires domains of the 10-15 nm for efficient exciton dissociation [35].

As shown in Fig. 8, XRD profile of the **1**: PC₇₁BM film processed without DIO shows only one broad band (weak) centered at $2\theta=4.15^\circ$, whereas the film processed with 4 % DIO/CB shows a sharp peak at $2\theta=4.15^\circ$ and higher order reflection at $2\theta=8.35^\circ$ and $2\theta=12.18^\circ$, indicating that the film processed with DIO/CB solvent has higher crystallinity. The decrease in d-spacing (estimated from the XRD peak around $2\theta=4.15^\circ$ is about 2.346 nm and 2.224 nm for CB and DIO/CB processed film) indicates that the interlayer interaction become stronger. The DIO additive substantively increases the intermolecular π - π packing interactions in the semiconducting small molecules in the BHJ film compared to film without solvent additive, inducing more phase-separated morphology as observed in AFM images.

The series resistance (R_s) represents the total resistance of the bulk active layer as well as contact resistance, while the shunt resistance (R_{sh}) is related to leakage current across the device. The reverse saturation current density (J_o) in the device is the minority charge carrier (hole) density which gives the qualitative measure of the electron-hole recombination at D/A interfaces or BHJ/Al interfaces [36]. The device based on solvent additives, both the R_s and R_{sh} decreases. The reduction in R_s is most likely due to the increase formation of crystalline zones and enhanced molecular ordering which consequently contributes to increase in carrier mobility or better charge extraction.

The value of V_{oc} was slightly reduced with the incorporation DIO additive. The V_{oc} of the BHJ solar cells depends on the energy offset between the HOMO of donor and LUMO of acceptor [37], the difference in the work functions of electrodes from metal-insulator- metal model [38] and the influence of surface dipoles [38]. The reduction in the V_{oc} has been commonly observed in polymers solar cells after thermal annealing and solvent annealing attributed to the improved crystalline ordering of polymer chain and molecular ordering [40], leading to the reduction of HOMO level of polymer. Therefore, we assume that the decrease

in V_{oc} with the incorporation of DIO leads to better crystallization of donor phase. The high boiling point of DIO and poor solubility of PC₇₁BM in DIO play an important role in the crystallization of donor phase.

To get information about the effect of DIO on the operation of these devices, we have studied the recombination mechanisms in the devices using the light intensity dependence of J- V characteristics under different illumination intensities for 1 mW/cm² to 100 mW/cm² and then extract the values of J_{sc} . The variation of J_{sc} with illumination intensity in log –log scale, and fitted to power law, is shown in Figure 9. In most of the organic solar cells, a power law dependence was observed, i. e. $J_{sc} \propto P_{in}^{\alpha}$. The exponential factor $\alpha=1$ is indicative of efficient sweep –out of charge carriers prior to recombination [41]. We have estimated the value of exponential factor (α) for the devices processed with and without DIO as 0.937 and 0.898, respectively. The value of α for the device processed from the DIO is closer to unity implies that the sweep-out of charge carrier is more effective. This is consistent with the balance charge transport as observed from the mobility measurements. The more deviation from $\alpha=1$ in the device processed with CB only suggests that the bimolecular recombination is more important in this device. An unbalanced hole and electron mobility in this device can also be attributed to the deviation of α value from unity.

Conclusions

We have synthesized two symmetrical planar star small molecules **DMM-TPA[DTS(FBTTh₃)₃] (1)** and **TPA[DTS(FBTTh₃)₃] (2)** and investigated them as donor materials along with PC₇₁BM as acceptor for the fabrication of solution processed BHJ organic solar cells. The solar cells based on **1** and **2** showed PCE of 2.87 and 2.51 %, respectively. The higher PCE for the device based on **1** as compared to **2** attributed to lower bandgap and higher hole mobility of **1** as compared to **2**. We have further investigated the influence of solvent additive (DIO) on the photovoltaic performance of the organic solar cells based on these two small molecules. We found that the PCE of the devices is significantly enhanced for the devices when solvent additive (4 % by volume) is used for film processing, resulting in over all PCE of 5.16 % and 4.70 % for **1** and **2**, respectively. We found that the active layer processed from CB only showed poor phase separation, due to the higher recombination and unbalanced charge transport, leading to the lower both J_{sc} and FF. However, the device processed with 4 % DIO yields favorable nanoscale morphology, in which phase separation is sufficiently created percolating pathway for charge transport. The

enhancement in the hole mobility for DIO/CB processed active layer also indicates a balance charge transport in the devices, resulting higher J_{sc} , FF and PCE.

Acknowledgment

This work was supported by the Converging Research Center Program through the Ministry of Science, ICT and Future Planning, Korea (2013K000203), the International Science and Business Belt Program through the Ministry of Education, Science and Technology (no. 2012K001573).

Reference

1. J. Peet, A. J. Heeger and G. C. Bazan, *Acc. Chem. Res.* 2009, **42**, 1700
2. (a) S. E. Shaheen, C. J. Brabec, N. S. Sariciftci, F. Padinger, T. Fromherz and J. C. Hummelen, *Appl. Phys. Lett.* 2001, **78**, 841, (b) Y. Liang, Z. Xu, J. Xia, S.-T. Tsai, Y. Wu, G. Li, C. Ray and L. Yu, *Adv. Mater.* 2010, **22**, E135
3. Z. He, C. Zhong, S. Su, M. Xu, H. Wu and Y. Cao, *Nat. Photonics* 2012, **6**, 591
4. (a) D. Mühlbacher, M. Scharber, M. Morana, Z. Zhu, D. Waller, R. Gaudiana and C. Brabec, *Adv. Mater.* 2006, **18**, 2884, (b) N. Blouin, A. Michaud, D. Gendron, S. Wakim, E. Blair, R. Neagu-Plesu, M. Belletête, G. Durocher, Y. Tao and M. Leclerc, *J. Am. Chem. Soc.* 2007, **130**, 732, (c) Y. Liang, Y. Wu, D. Feng, S.-T. Tsai, H.-J. Son, G. Li and L. Yu, *J. Am. Chem. Soc.* 2008, **131**, 56, (d) Y. He, H.-Y. Chen, J. Hou and Y. Li, *J. Am. Chem. Soc.* 2010, **132**, 1377, (e) L. Lu, T. Xu, W. Chen, J. M. Lee, Z. Luo, I. H. Jung, H. I. Park, S. O. Kim and L. Yu, *Nano Lett.* 2013, **13**, 2365
5. (a) M. A. Green, K. Emery, Y. Hishikawa, W. Warta and E. D. Dunlop, *Prog. Photovoltaics* 2013, **21**, 827, (b) G. Li, R. Zhu and Y. Yang, *Nat. Photonics* 2012, **6**, 153, (c) S. H. Park, A. Roy, S. Beaupre, S. Cho, N. Coates, J. S. Moon, D. Moses, M. Leclerc, K. Lee and A. J. Heeger, *Nat. Photonics* 2009, **3**, 297, (d) R. F. Service, *Science* 2011, **332**, 293
6. (a) Y. Sun, G. C. Welch, W. L. Leong, C. J. Takacs, G. C. Bazan and A. J. Heeger, *Nat. Mater.* 2012, **11**, 44–48, (b) A. K. K. Kyaw, D. H. Wang, V. Gupta, J. Zhang, S. Chand, G. C. Bazan and A. J. Heeger, *Adv. Mater.* 2013, **25**, 2397–2402, (c) Y. Liu, X. Wan, F. Wang, J. Zhou, G. Long, J. Tian, J. You, Y. Yang and Y. Chen, *Adv. Energy Mater.* 2011, **1**, 771–775, (d) J. Huang, C. Zhan, X. Zhang, Y. Zhao, Z. Lu, H. Jia, B. Jiang, J. Ye, S. Zhang, A. Tang, Y. Liu, Q. Pei and J. Yao, *ACS Appl. Mater. Interfaces*, 2013, **5**, 2033, (e) T. S. van der Poll, J. A. Love, T.-Q. Nguyen and G. C. Bazan, *Adv. Mater.* 2012, **24**, 3646
7. (a) J. Zhou, Y. Zuo, X. Wan, G. Long, Q. Zhang, W. Ni, Y. Liu, Z. Li, G. He, C. Li, B. Kan, M. Li and Y. Chen, *J. Am. Chem. Soc.* 2013, **135**, 8484–8487, (b) Aung Ko Ko Kyaw, Dong Hwan Wang, Chan Luo, Yong Cao, Thuc-Quyen Nguyen, Guillermo C. Bazan, and Alan J. Heeger, *Adv. Energy Mater.* 2013, **25**, 2397, (c) V. Gupta, A. K. K. Kyaw, D. H. Wang, S. Chand, G. C. Bazan and A. J. Heeger, *Sci. Rep.*, 2013, **3**, 1965

8. (a) H. X. Shang, H. J. Fan, Y. Liu, W. P. Hu, Y. F. Li and X. W. Zhan, *Adv. Mater.* 2011, **23**, 1554, (b) S. Haid, A. Mishra, M. Weil, C. Urich, M. Pfeiffer and P. Bäuerle, *Adv. Funct. Mater.* 2012, **22**, 4322, (c) J. Y. Zhou, X. J. Wan, Y. S. Liu, Y. Zuo, Z. Li, G. R. He, G. K. Long, W. Ni, C. X. Li, X. C. Su and Y. S. Chen, *J. Am. Chem. Soc.* 2012, **134**, 16345, (d) Z. Li, G. R. He, X. J. Wan, Y. S. Liu, J. Y. Zhou, G. K. Long, Y. Zou, M. T. Zhang and Y. S. Chen, *Adv. Energy Mater.* 2012, **2**, 74
9. S. A. Ponomarenko, S. Kirchmeyer, A. Elschner, B. Huisman, A. Karbach and D. Drechsler, *Adv. Funct. Mater.* 2003, **13**, 591
10. (a) S. Roquet, A. Cravino, P. Leriche, O. Aleveque, P. Free and J. Roncali, *J. Am. Chem. Soc.* 2006, **128**, 3459, (b) E. Ripaud, T. Rousseau, P. Leriche and J. Roncali, *Adv. Energy Mater.* 2011, **1**, 540, (c) D. Deng, S. L. Shen, J. Zhang, C. He, Z. J. Zhang and Y. F. Li, *Org. Electron.* 2012, **13**, 2546, (d) J. Zhang, Y. Yang, C. He, Y. J. He, G. J. Zhao and Y. F. Li, *Macromolecules* 2009, **42**, 7619, (e) Jie Min, Yuriy N. Luponosov, Andreas Gerl, Marina S. Polinskaya, Svetlana M. Peregodova, Petr V. Dmitryakov, Artem V. Bakirov, Maxim A. Shcherbina, Sergei N. Chvalun, Souren Grigorian, Nina Kaush-Busies, Sergei A. Ponomarenko, Tayebbeh Ameri, and Christoph J. Brabec, *Adv. Energy mater.* doi: 10.1002/aenm.201301234
11. Y. Sun, G.C. Welch, W.L. Leong, C.J. Takacs, G.C. Bazan and A.J. Heeger, *Nat. Mater.* 2012, **11**, 44-48.
12. S. Park, N. Cho, S. Cho, J.K. Lee and J. Ko, *Org. Lett.* 2012, **14**, 6329-6329
13. (a) H. M. Ko, H. Choi, S. Paek, K. Kim, K. Song, J. K. Lee and J. Ko, *J. Mater. Chem.* 2011, **21**, 7248–7253; (b) B. S. Jeong, H. Choi, N. Cho, H. M. Ko, W. Lim, K. Song, J. K. Lee and J. Ko, *Sol. Energy Mater. Sol. Cells* 2011, **95**, 1731–1740; (c) S. So, H. Choi, C. Kim, N. Cho, H. M. Ko, J. K. Lee and J. Ko, *Sol. Energy Mater. Sol. Cells* 2011, **95**, 3433–3441; (d) S. So, H. Choi, H. M. Ko, C. Kim, S. Paek, N. Cho, K. Song, J. K. Lee and J. Ko, *Sol. Energy Mater. Sol. Cells* 2012, **98**, 224–232; (e) H. Choi, S. Paek, J. Song, C. Kim, N. Cho and J. Ko, *Chem. Commun.* 2011, **47**, 5509–5511, (f) J. K. Lee, B. S. Jeong, J. Kim, C. Kim and J. Ko, *J. Photochem. Photobiol. A: Chemistry* 2013, **251**, 25-32, (g) S. Paek, J.W. Lee and J. Ko, *Sol. Energy Mater. Sol. Cells*, 2014, **120**, 209-2171
14. (a) J. Lee, M. H. Yun, J. Kim, J. Y. Kim and C. Yang, *Macromol. Rapid Commun.* 2012, **33**, 140–145; (b) J. Lee, J. Kim, G. Kim and C. Yang, *Tetrahedron* 2010, **66**, 9440–9444.
15. (a) H. Zhou, L. Yang, A. C. Stuart, S. C. Price, S. Liu and W. You, *Angew. Chem.* 2011, **123**, 3051–3054; *Angew. Chem. Int. Ed.* 2011, **50**, 2995–2998, (b) Y. Zhang, S. C. Chien, K. S. Chen, H. L. Yip, Y. Sun, J. A. Davices, F. C. Chen and A. K. Y. Jen, *Chem. Commun.* 2011, **47**, 11026–11028, (c) Y. Y. Liang, D. Q. Feng, Y. Wu, S. T. Tsai, G. Li, C. Ray and L. P. Yu, *J. Am. Chem. Soc.* 2009, **131**, 7792–7799; (d) Q. Wei, T. Nishizawa, K. Tajima and K. Hashimoto, *Adv. Mater.* 2008, **20**, 2211–2216
16. Nara Cho, Kihyung Song, Jae Kwan Lee, and Jaejung Ko, *Chem. Eur. J.* 2012, **18**, 11433–11439

17. S. Paek, N. Cho, S. Cho, S. Lee and J. K; Ko, *J. Org. Lett.*, 2012, **14**, 6326-6329
18. (a) G. Malliaras, J. Salem, P. Brock and C. Scott, *Phys. Rev. B* 1998, **58**, 13411, (b) H. Martens, H. Brom and P. Blom, *Phys. Rev. B* 1999, **60**, 8489
19. (a) W. Ma, C. Yang, X. Gong, K. Lee and A. J. Heeger, *Adv. Funct. Mater.* 2005, **15**, 1617, (b) X. Yang, J. Loos, S. C. Veenstra, W. J. H. Verhees, M. M. Wienk, J. M. Kroon, M. A. J. Michels and R. A. J. Janssen, *Nano Lett.* 2005, **5**, 579.
20. (a) G. Li, V. Shrotriya, J. Huang, Y. Yao, T. Moriarty, K. Emery and Y. Yang, *Nat. Mater.* 2005, **4**, 864, (b) G. Li, Y. Yao, H. Yang, V. Shrotriya, G. Yang and Y. Yang, *Adv. Funct. Mater.* 2007, **17**, 1636.
21. (a) J. S. Moon, C. J. Takacs, Y. Sun and A. J. Heeger, *Nano Lett.* 2011, **11**, 1036, (b) D. H. Wang, J. S. Moon, J. Seifter, J. Jo, J. H. Park, O. O. Park and A. J. Heeger, *Nano Lett.* 2011, **11**, 3163
22. (a) Y. Yao, J. Hou, Z. Xu, G. Li and Y. Yang, *Adv. Funct. Mater.* 2008, **18**, 1783, (b) J. S. Moon, C. J. Takacs, S. Cho, R. C. Coffin, H. Kim, G. C. Bazan and A. J. Heeger, *Nano Lett.* 2010, **10**, 4005, (c) J. Peet, J. Y. Kim, N. E. Coates, W. L. Ma, D. Moses, A. J. Heeger and G. C. Bazan, *Nat. Mater.* 2007, **6**, 497
23. (a) H.-Y. Chen, H. Yang, G. Yang, S. Sista, R. Zadoyan, G. Li and Y. Yang, *J. Phys. Chem. C* 2009, **113**, 7946, (b) J. Peet, C. Soci, R. C. Coffin, T. Q. Nguyen, A. Mikhailovsky, D. Moses and G. C. Bazan, *Appl. Phys. Lett.* 2006, **89**, 252105
24. (a) A. K. K. Kyaw, D. H. Wang, D. Wynands, J. Zhang, T.-Q. Nguyen, G. C. Bazan and A. J. Heeger, *Nano. Lett.* 2013, **13**, 3796, (b) Aung Ko Ko Kyaw, Dong Hwan Wang, Chan Luo, Yong Cao, Thuc-Quyen Nguyen, Guillermo C. Bazan and Alan J. Heeger, *Adv. Energy Mater.* doi: 10.1002/aenm.201301469
25. (a) J.A. Love, C.M. Proctor, J. Liu, C. J. Takacs, A. Sharenko, T.S. van der Poll, A.J. Heeger, G.C. Bazan and T.Q. Nguyen, *Adv. Funct. Mater.* 2013, **23**, 5019–502, (b) C. J. Takacs, Y. Sun, G.C. Welch, L.A. Perez, X. Liu, W. Wen, G. C. Bazan and A. J. Heeger, *J. Am. Chem. Soc.* 2012, **134**, 16597–16606.
26. S. R. Cowan, R. A. Street, S. Cho and A. J. Heeger, *Phys. Rev. B* 2011, **83**, 035205
27. (a) D. Di Nuzzo, S. van Reenen, R.A. J. Janssen, M. Kemerink and S. C. J. Meskers, *Phys. Rev. B* 2013, **87**, 085207, (b) V. D. Mihailetschi, J. Wildeman and P.W. M. Blom, *Phys. Rev. Lett.* 2005, **94**, 126602
28. V. Coropceanu, J. Cornil, D.A. da Silva Filho, Y. Olivier, R. Silbey and J. L. Bré das, *Chem. Rev.* 2007, **107**, 926–952
29. (a) N. Ueno, In *Semiconducting Polymer Composites: Principles, Morphologies, Properties and Applications*; Yang, X., Ed.; John Wiley & Sons: Weinheim, Germany, 2012, (b) S. Scheinert, M. Grobosch, J. Sprogies, I. Hörselmann, M. Knupfer and G. Paasch, *J. Appl. Phys.* 2013, **113**, 174504

30. (a) A. Pivrikas, N.S. Sariciftci, G. Juška and R. Österbacka, *Prog. Photovoltaics* 2007, **15**, 677–696. (b) C. M. Proctor, M. Kuik, T. Q. Nguyen, *Prog. Polym. Sci.* 2013, **38**, 1941–1960.
31. V. D. Mihailetschi, L. J. A. Koster, J. C. Hummelen and P.W.M. Blom, *Phys. Rev. Lett.* 2004, **93**, 216601
32. Q. Peng, X. Liu, Y. Qin, D. Zhou and J. Xu, *J. Polym. Sci. Part A* 2011, **49**, 4458–4467
33. A. K. K. Kyaw, D. H. Wang, C. Luo, Y. Cao, T. Q. Nguyen, G. C. Bazan and A. J. Heeger, *Adv. Energy Mater.* doi: 10.1002/aenm.201301469
34. S.J. Lou, J. M. Szarko, T. Xu, L. Yu, T. J. Marks and L. X. Chen, *J. Am. Chem. Soc.* 2011, **133**, 20661–20663.
35. B. P. Lyons, N. Clarke and C. Groves, *Energy Environ. Sci.* 2012, **5**, 7657–7663
36. C. Waldauf, M. C. Scharber, P. Schilinsky, J. A. Hauch and C. J. Brabec, *J. Appl. Phys.* 2006, **99**, 104503
37. C. J. Brabec, A. Cravino, D. Meissner, N. S. Sariciftci, T. Fromherz, M. T. Rispens, L. Sanchez and J. C. Hummelen, *Adv. Funct. Mater.* 2001, **11**, 374
38. I. D. Parker, *J. Appl. Phys.* 1994, **75**, 1656
39. G. Li, C.-W. Chu, V. Shrotriya, J. Huang and Y. Yang, *Appl. Phys. Lett.* 2006, **88**, 253503
40. (a) F. Padinger, R. S. Rittberger and N. S. Sariciftci, *Adv. Funct. Mater.* 2003, **13**, 85, (b) W. Ma, C. Yang, X. Gong, K. Lee and A. J. Heeger, *Adv. Funct. Mater.* 2005, **15**, 1617
41. (a) P. Schilinsky, C. Waldauf and C. J. Brabec, *Appl. Phys. Lett.* 2002, **81**, 3885, (b) J. K. J. van Duren, X. Yang, J. Loos, C. W. T. Bulle-Lieuwma, A. B. Sieval, J. C. Hummelen and R. A. J. Janssen, *Adv. Funct. Mater.* 2004, **14**, 425

Table 1. Optical, redox parameters of the compounds

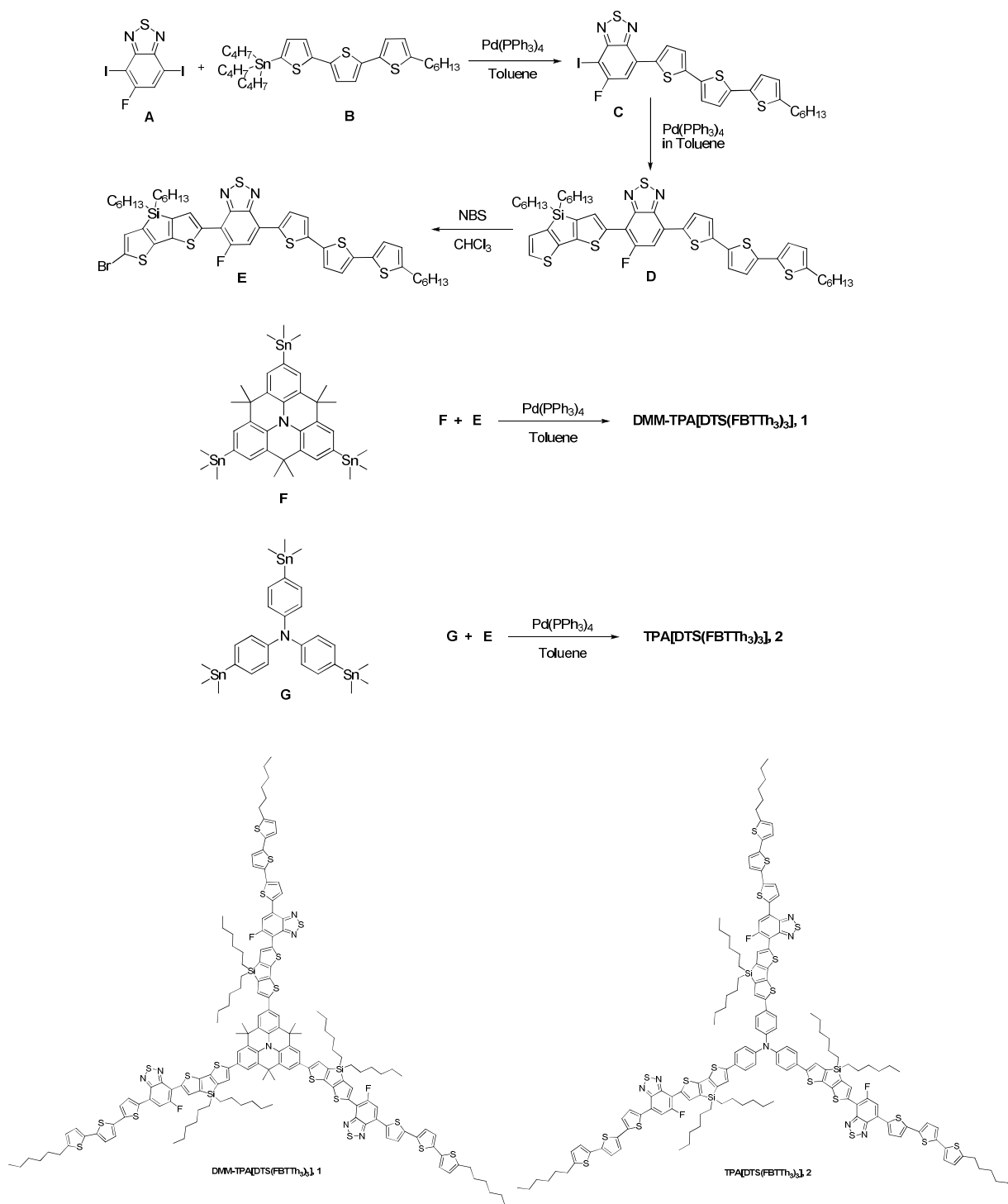
Compounds	$\lambda_{\text{abs}}^{[a]}$ (nm) ($\epsilon/M^{-1}\text{cm}^{-1}$)	$\lambda_{\text{PL}}^{[a]}$ (nm)	$E_{\text{onset, ox}}(\text{V})$ /HOMO (eV) ^[b]	$E_{\text{onset, red}}(\text{V})$ / LUMO (eV) ^[b]	$E_{\text{elec}}(\text{eV})^{\text{[b]}}$	$E_{\text{opt}}(\text{eV})$	$E_{\text{g}}(\text{eV})^{\text{[d]}}$
1	413 (77,500), 575 (98,100)	737	0.0381/ -4.8381	-1.056 / -3.744	1.094	1.61	1.83
2	406 (102,000), 564 (120,000)	730	0.0869/ -4.8869	1.3429 / -3.4571	1.4298	1.73	1.86

[a] Absorption spectra were measured in chlorobenzene solution. [b] Redox potential of the compounds were measured in CH_2Cl_2 with 0.1M $(n\text{-C}_4\text{H}_9)_4\text{NPF}_6$ with a scan rate of 50 mVs^{-1} (vs. Fc/Fc^+).

Table 2. Photovoltaic parameters of the BHJ solar cells with different active layers

Blend	$J_{\text{sc}} (\text{mA}/\text{cm}^2)$	$V_{\text{oc}} (\text{V})$	FF	PCE (%)
1:PC ₇₁ BM (1:2) ^a	9.18	0.68	0.46	2.87
2:PC ₇₁ BM (1:2) ^a	8.54	0.70	0.42	2.51
1:PC ₇₁ BM (1:2) ^b	12.62	0.66	0.62	5.16
2:PC ₇₁ BM (1:2) ^b	11.92	0.68	0.58	4.70

^acast from CB, ^bcast from DIO (4 %v)/ CB



Scheme 1. Schematic diagram for the synthesis of the two compounds

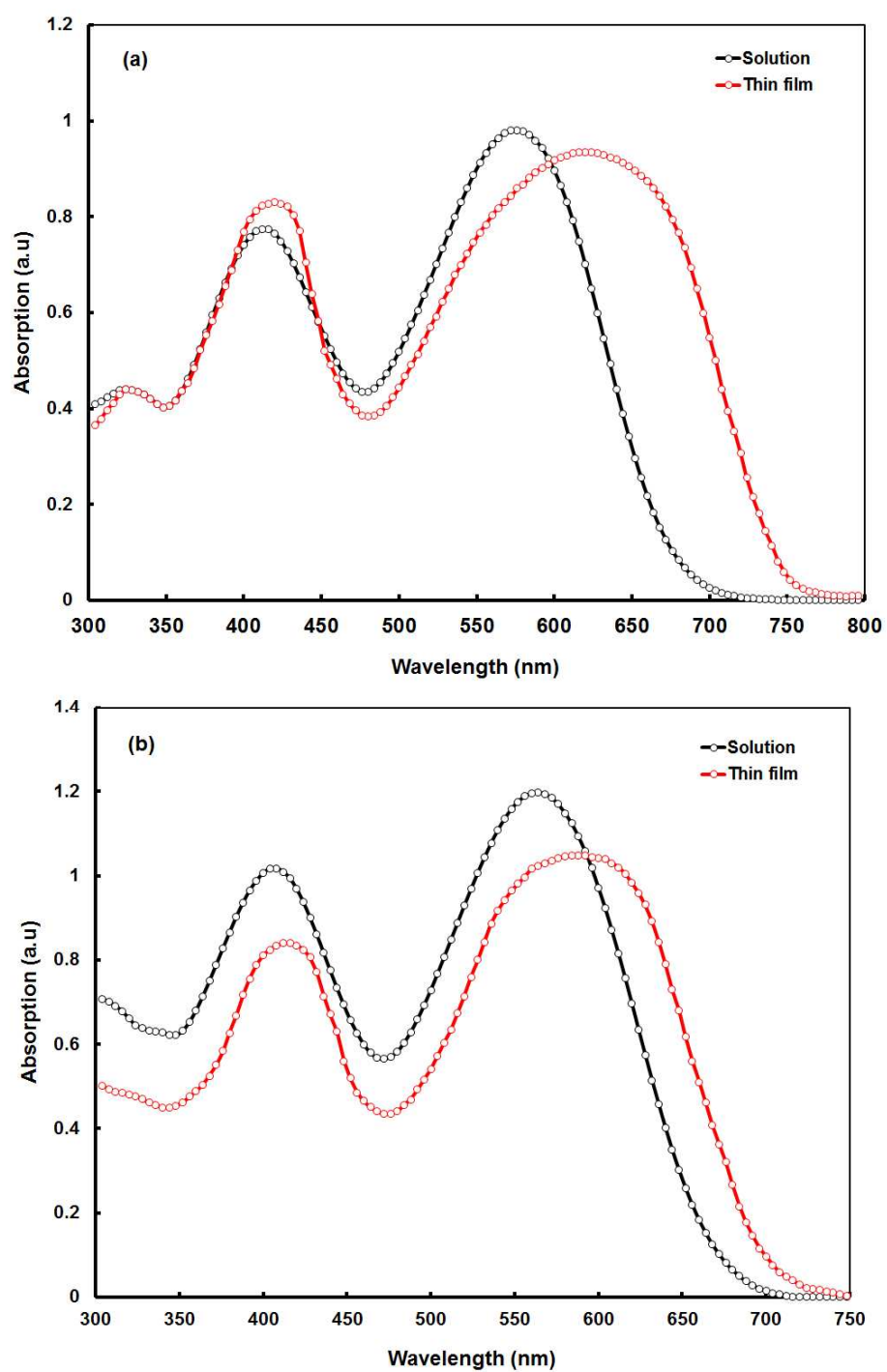


Figure 1. Optical absorption spectra of (a) 1 and (b) 2 in solution and thin film form.

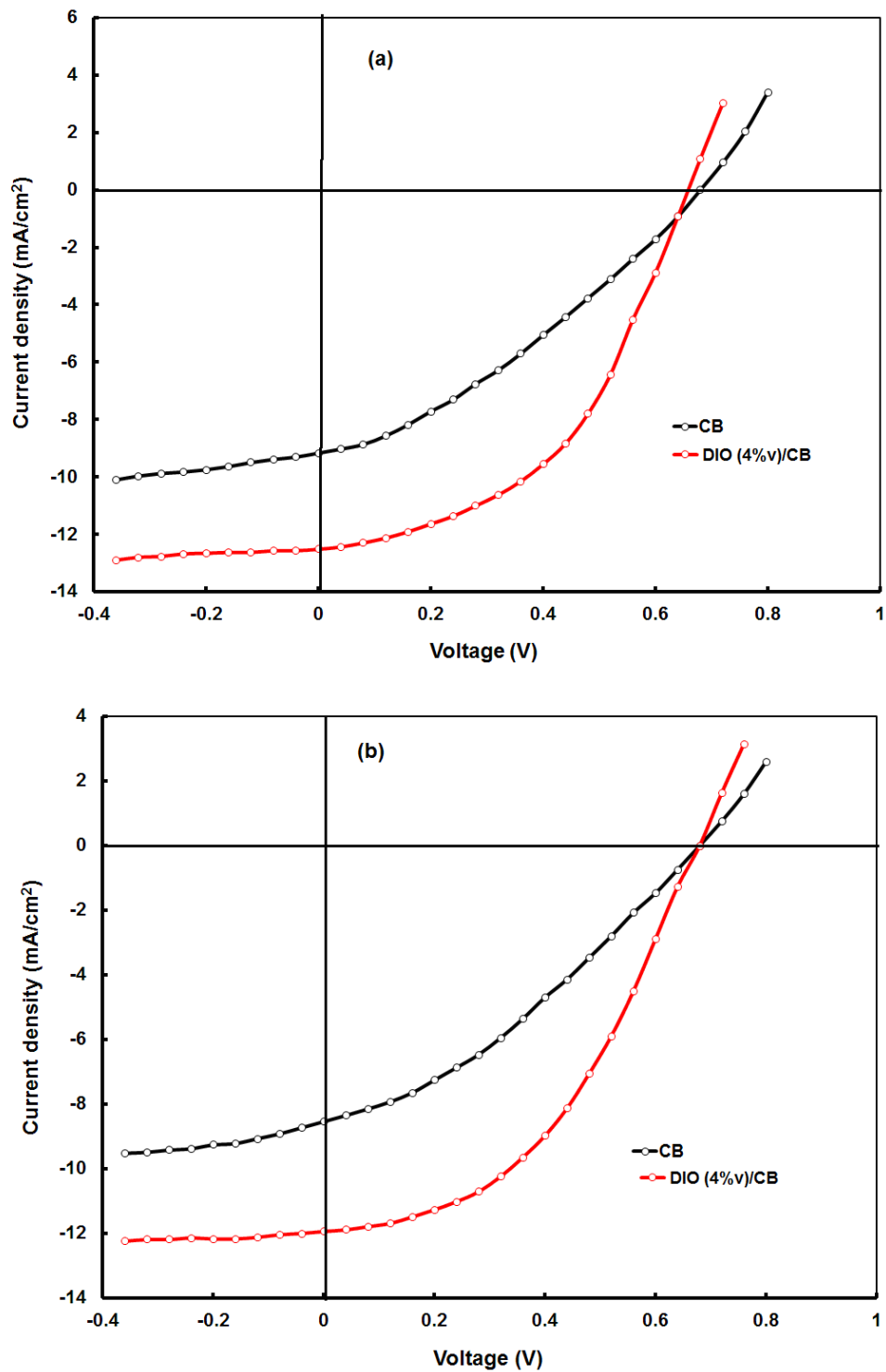


Figure 2. Current –voltage characteristics under illumination for the devices (a) 1:PC₇₁BM (1:2) and (b) 2:PC₇₁BM (1:2) active layers

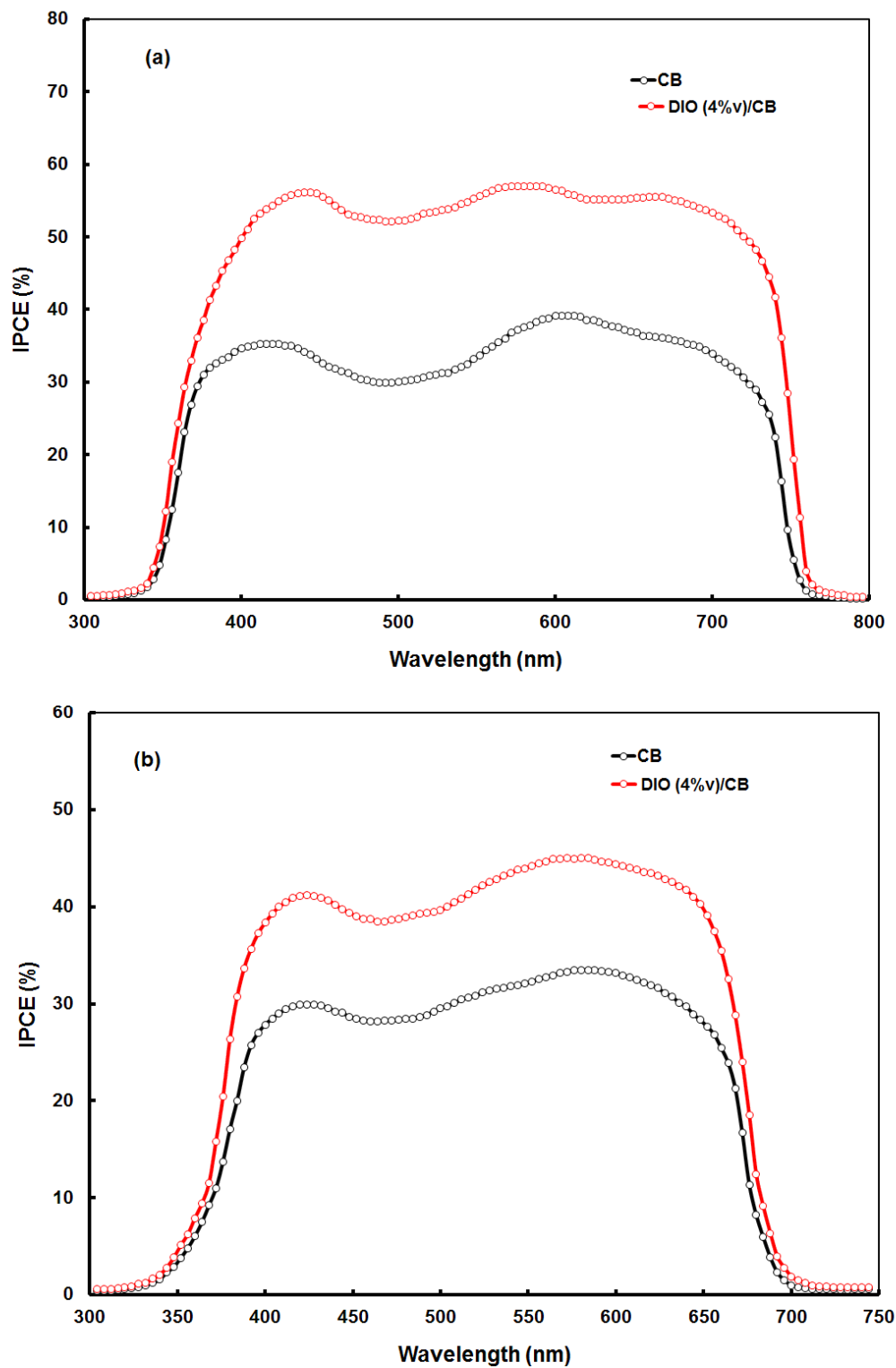


Figure 3. IPCE spectra of the devices based on (a) 1:PC₇₁BM and (b) 2:PC₇₁BM active layers

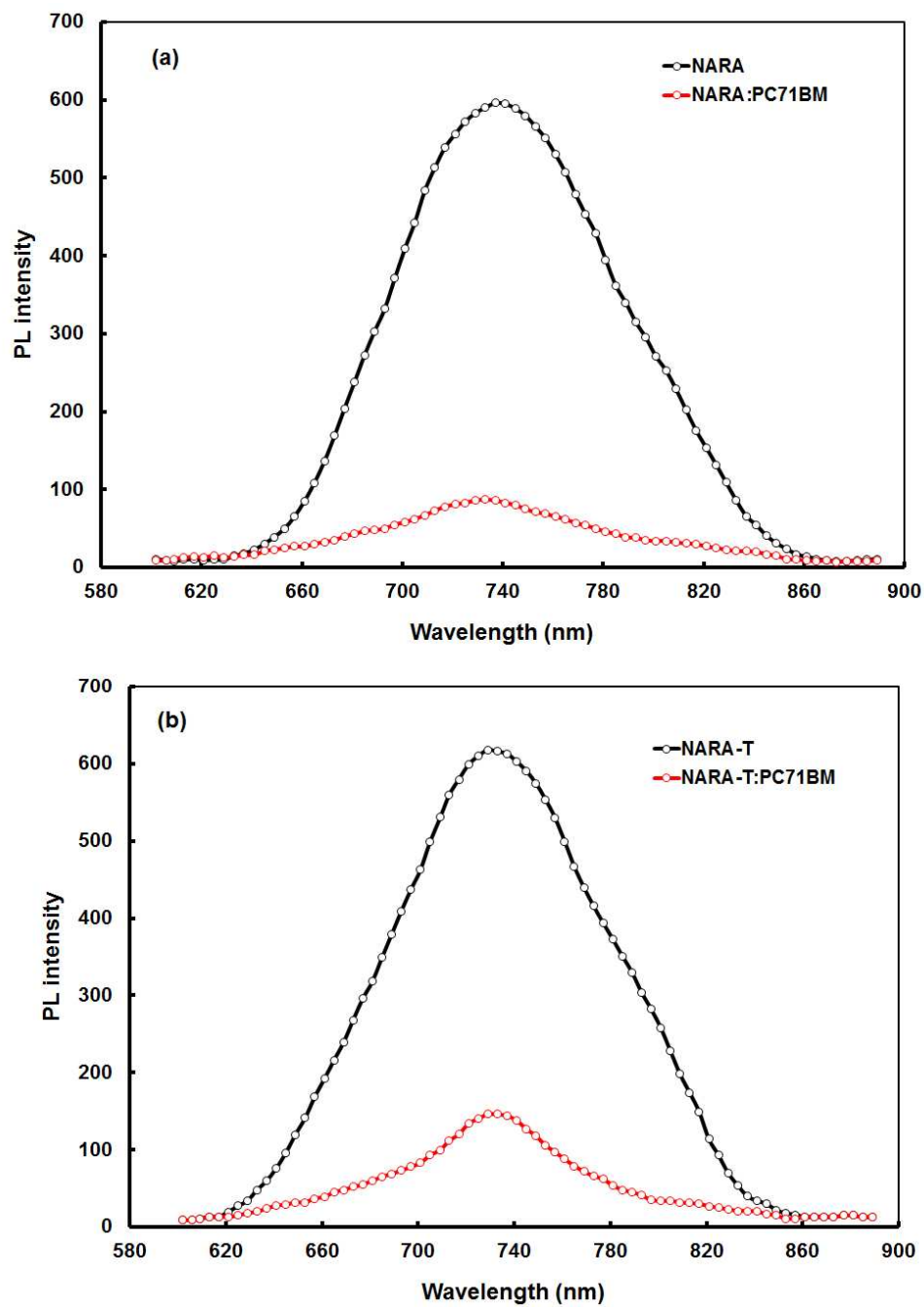


Figure 4. Photoluminescence (PL) of (a) **1** and **1:PC₇₁BM** and (b) **2** and **2:PC₇₁BM**

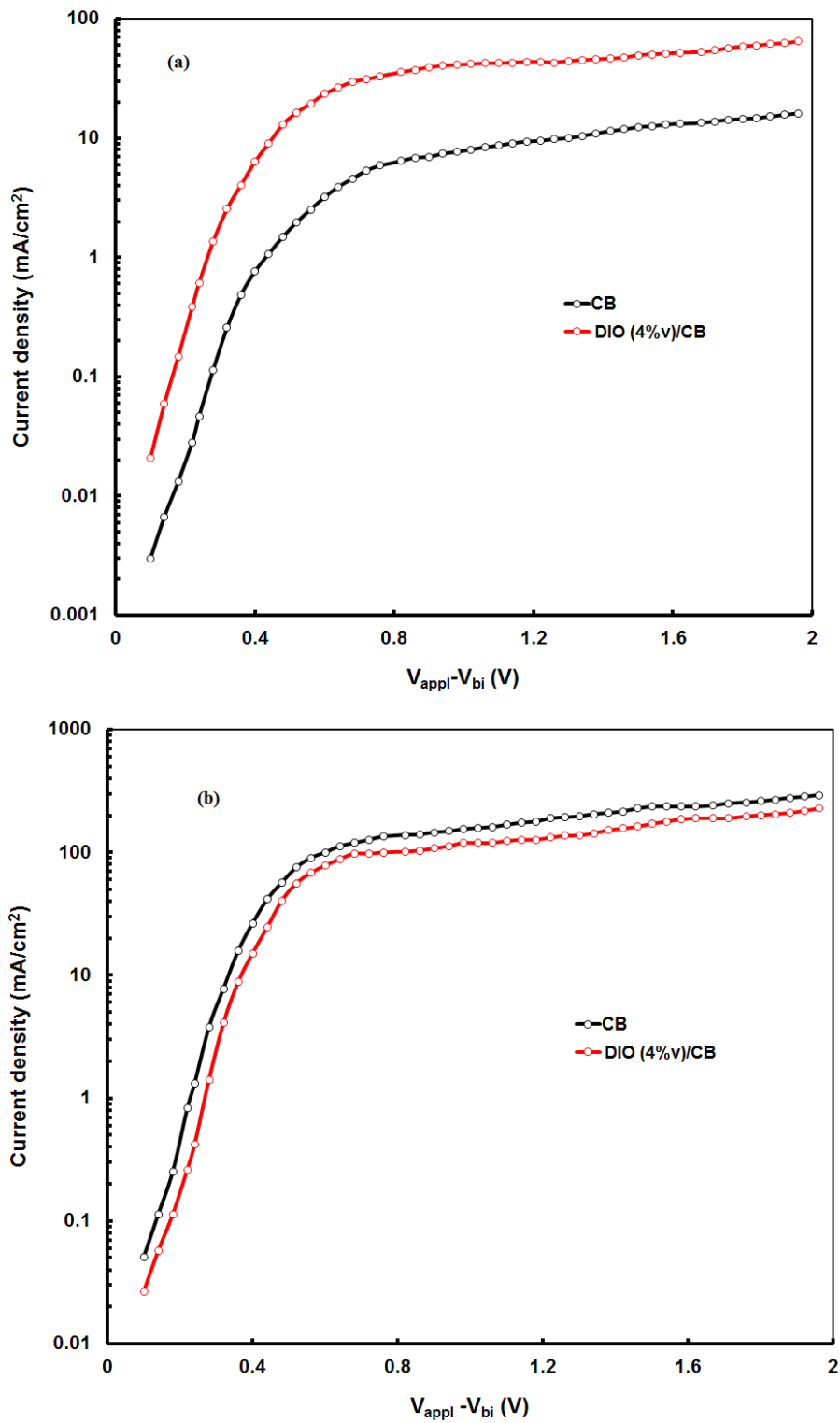


Fig. 5. J-V characteristics in dark of (a) hole only devices and (b) electron only devices based on 1:PC₇₁BM processed with and without DIO additives

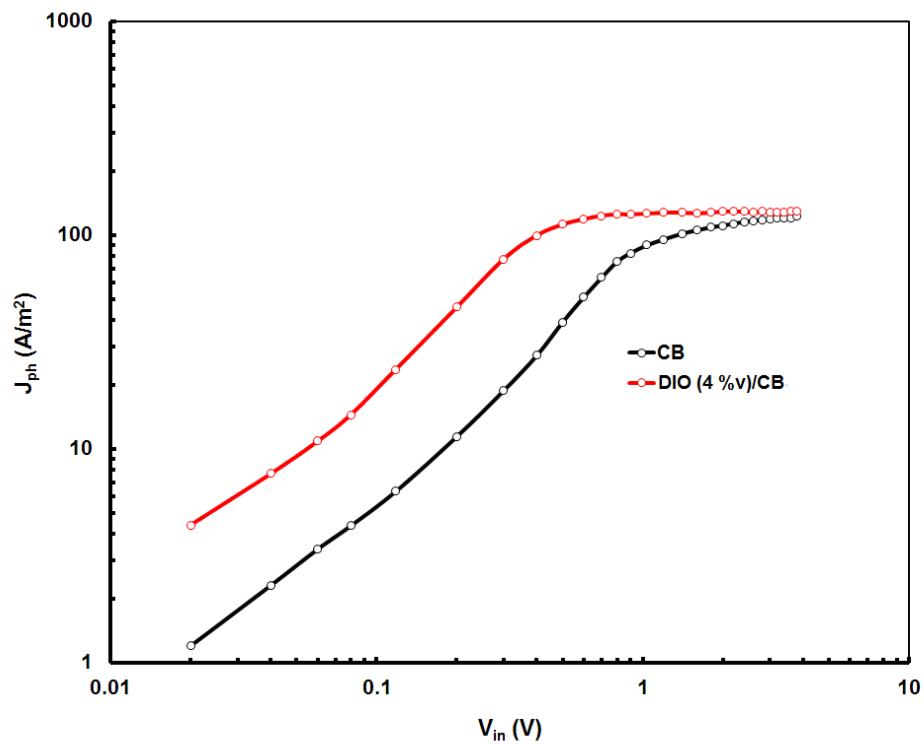


Fig. 6. Photocurrent density (J_{ph}) variation with internal voltage (V_{in}) for 1:PC₇₁BM devices processed with and without DIO additives

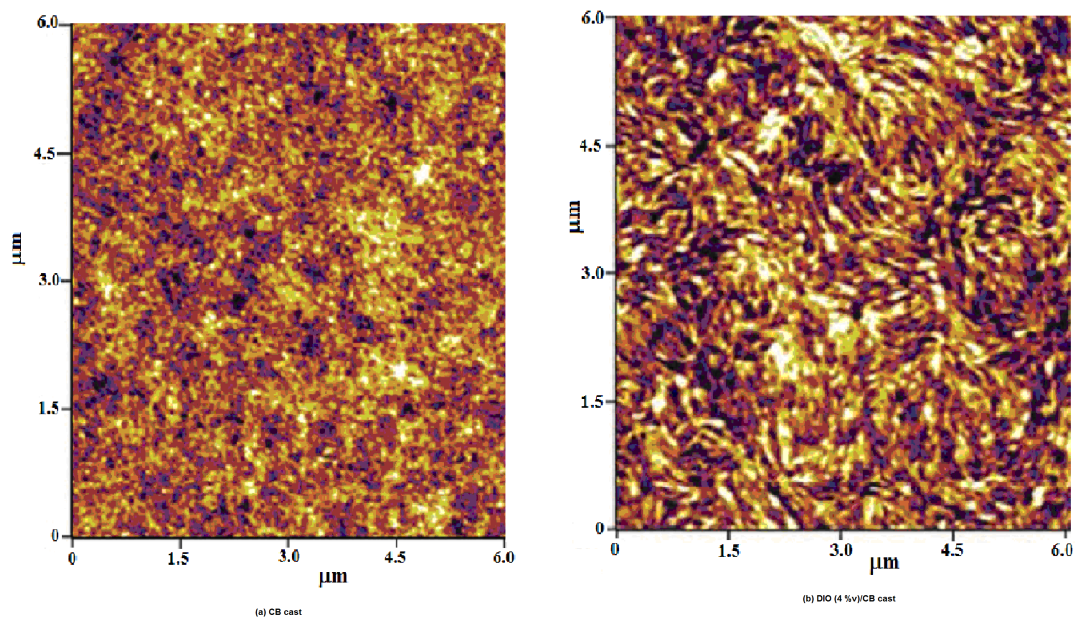


Fig. 7. AFM images of 1: PC₇₁BM films processed with and without DIO additives

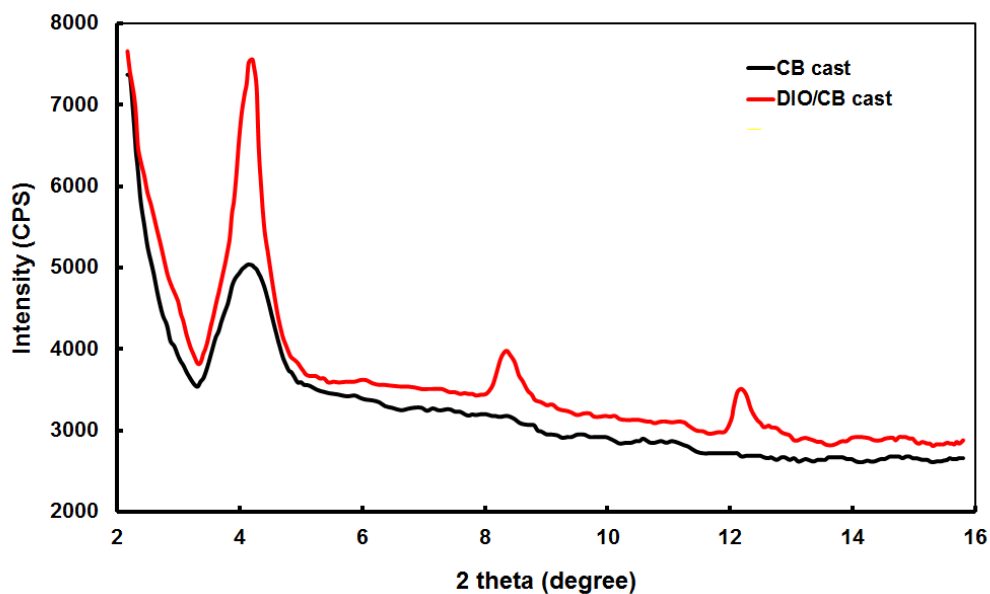


Fig. 8. XRD patterns of the 1:PC₇₁BM films processed with and without DIO additive

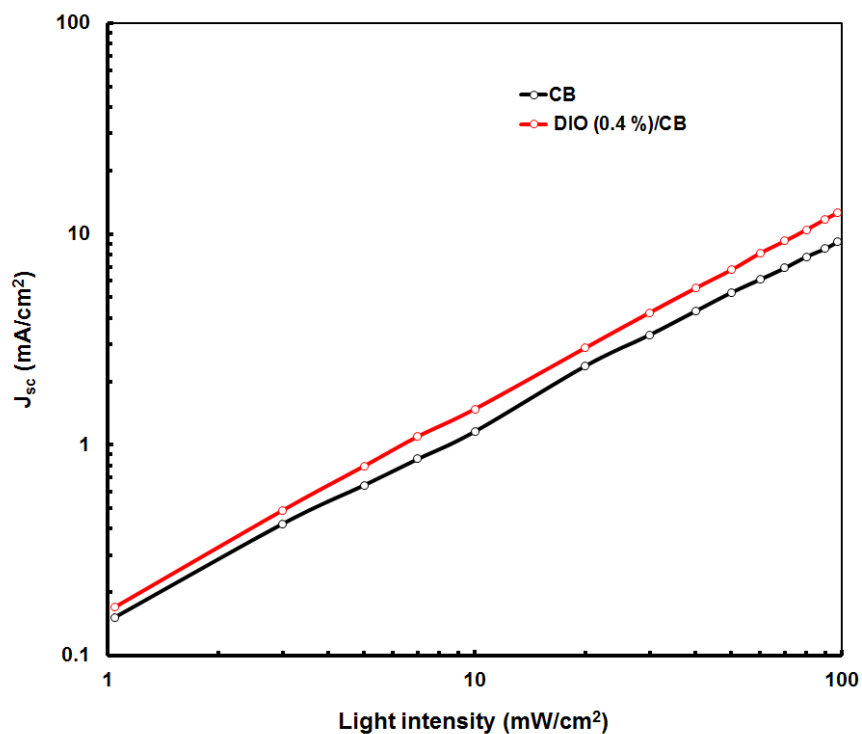


Fig. 9. Variation of the J_{sc} with illumination intensity of 1:PC₇₁BM solar cells processed with and without DIO additive

Synthesis, optical and electrochemical properties of small molecules DMM-TPA[DTS(FBTTh₃)₃] and TPA[DTS(FBTTh₃)₃] and their application as donors for bulk heterojunction solar cells

Nara Cho,^a Sanhhyun Paek,^a Jihye Jeon,^b Kihyung Song,^b G. D. Sharma,^{*c} and Jaejung Ko^{*a}

Two organic small molecules DMM-TPA[DTS(FBTTh₃)₃] (**1**) and TPA[DTS(FBTTh₃)₃] (**2**) were synthesized and characterized and used donor along with PC₇₁BM for the use in solution processed bulk heterojunction solar cells. The PCE of the solution processed BHJ solar cells was improved up to 5.16 % and 4.70% for **1** and **2**, respectively, when active layers were processed with 0.4 % DIO as additive in the CB solvent. The enhancement in the PCE was mainly due to the increase in J_{sc} and FF. The increase in the J_{sc} and FF is attributed to the balance charge transport between the electron and hole transport and reduction in the bimolecular recombination, leading to an increase in the PCE.

